Role of Indenter Material and Size in Veneer Failure of Brittle Layer Structures

Sanjit Bhowmick,[1] Juan José Meléndez-Martínez,[2] Ilja Hermann,[1] Yu Zhang,[3] Brian R. Lawn[1]

[1] Materials Science and Engineering Laboratory, National Institute of Standards and Technology, Gaithersburg, Maryland 20899-8500

[2] Departamento de Física, Facultad de Ciencias, Universidad de Extremadura, 06071 Badajoz, Spain

[3] Department of Biomaterials and Biomimetics, New York University College of Dentistry, New York, New York 10010

Received 17 July 2006; revised 8 September 2006; accepted 13 September 2006
Published online 20 December 2006 in Wiley InterScience (www.interscience.wiley.com). DOI: 10.1002/jbm.b.30728

Abstract: The roles of indenter material and size in the failure of brittle veneer layers in all-ceramic crown-like structures are studied. Glass veneer layers 1 mm thick bonded to alumina layers 0.5 mm thick on polycarbonate bases (representative of porcelain/ceramic-core/dentin) are subject to cyclic contact loading with spherical indenters in water (representative of occlusal biting environment). Two indenter materials—glass and tungsten carbide—and three indenter radii—1.6, 5.0, and 12.5 mm—are investigated in the tests. A video camera is used to follow the near-contact initiation and subsequent downward propagation of cone cracks through the veneer layer to the core interface, at which point the specimen is considered to have failed. Both indenter material and indenter radius have some effect on the critical loads to initiate cracks within the local Hertzian contact field, but the influence of modulus is weaker. The critical loads to take the veneer to failure are relatively insensitive to either of these indenter variables, since the bulk of the cone crack propagation takes place in the contact far field. Clinical implications of the results are considered, including the issue of single-cycle overload versus low-load cyclic fatigue and changes in fracture mode with loading conditions.
 J Biomed Mater Res Part B: Appl Biomater 82B: 253–259, 2007

Keywords: cone cracks; dental crowns; cyclic fatigue; indenter size; indenter material

INTRODUCTION

In a series of preceding papers we described a competition between various near-contact fracture modes in crown-like brittle layer configurations subject to cyclic loading with hard spheres, in simulation of occlusal contact loading in dental function. Model flat-layer structures were used to elucidate the failure mechanisms, incorporating transparent materials to enable *in situ* viewing of crack evolution: monolith glass blocks, for control tests on a prototypical brittle material[1]; bilayers consisting of glass plates bonded to plastic substrates, representing single-layer dental crowns[2]; and trilayers consisting of glass plates fused to a stiff support ceramic in turn bonded to a plastic substrate, representing a veneer/core all-ceramic crown.[3] In these studies, the indenting sphere was a relatively hard material (WC), of relatively small fixed radius (1.6 mm). This choice of hard material was simply to enable multiple testing without the need for test-by-test replacement of the indenter; the choice of small radius was to ensure that failure initiated within the near-contact zone, in order to quantify veneer properties. Fractures consisted of outer and inner cone cracks and median cracks, Figure 1. Outer cone cracks are driven exclusively by Hertzian contact stresses, in conjunction with moisture-assisted slow crack growth. Inner cone and median cracks are also subject to contact stresses and slow crack growth, but are respectively augmented by hydraulic pumping in aqueous environments and cumulative elastic–plastic residual stress fields, making them particularly susceptible to fatigue. Failure is deemed to occur when any one of these cracks fully traverses the thickness of the outermost, brittle veneer layer.

Noting that occlusal contacts on real porcelain crown veneers are generally made with opposing tooth enamel of like modulus and relatively large cuspal radius,[4] the clinical relevance of such a model testing configuration has been questioned.[5] How is the evolution of top-surface cracks

Correspondence to: Brian Lawn (e-mail: brian.lawn@nist.gov)
Contract grant sponsor: National Institute of Dental and Craniofacial Research; contract grant number: PO1 DE10976

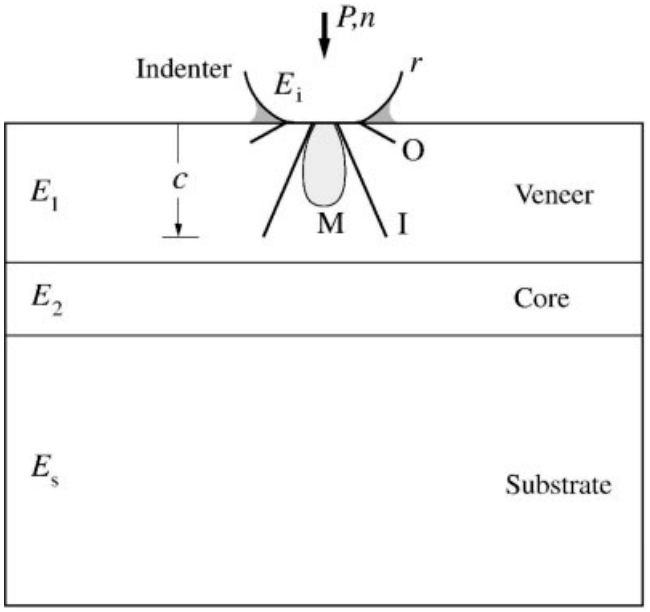

Figure 1. Schematic of crack geometry for cyclic contact on brittle veneer/core layer bonded to compliant support base with sphere of radius r at load P for number of cycles n in water (shaded). Showing top-surface veneer crack modes of characteristic through-thickness depth c: outer cone cracks (O), inner cone cracks (I), and median cracks (M). Inner and median cracks are sometimes hard to distinguish in glass, so any M data are collectively lumped in with I data in subsequent figures.

affected by going to more realistic occlusal conditions? Generally, it might be expected that more compliant and larger indenters will inhibit crack initiation, if only by virtue of a diminished stress intensity in the contact field. In extreme cases, depending on the thickness of the brittle layers and crown curvature, the fracture source may shift to crown subsurfaces[6] or even margins.[7] While these latter can become dominant failure modes, they are less dependent on indenter near-field characteristics, and will not be addressed explicitly here.

Accordingly, in this paper we address the role of indenter characteristics in top-surface crack evolution by conducting cyclic fatigue tests in water with WC and glass indenters of radii 1.6, 5.0, and 12.5 mm on a structure consisting of 1 mm glass veneer fused onto a 0.5 mm alumina core ceramic, all bonded to a thick polycarbonate base. This trilayer structure simulates the essential layer structure of an all-ceramic crown. The use of glass indenters meets the requirement for like modulus between opposing occlusal contacts, since its modulus is close to that of tooth enamel and crown porcelain. Alumina is a typical all-ceramic core material. The indenter radii cover a range of cuspal curvatures.[4] We will demonstrate that the cone fracture evolution from initiation to final failure is only mildly sensitive to indenter material, provided the indenter modulus remains at least as hard as the veneer material. The influence of indenter radius is somewhat stronger, especially in the initiation stages within the near-contact field. Clinical implications of the results in the context of single-cycle overload versus long-term fatigue are discussed.

EXPERIMENTAL

A trilayer specimen configuration used in an earlier study was retained for the current tests.[3] Soda-lime glass plates $25 \times 25 \times 1$ mm^3 with polished side surfaces for subsequent side-on viewing were fused at 600°C onto alumina plates $12 \times 12 \times 0.5$ mm^3 (AD995, CoorsTek, Golden, CO) using thin (<50 μm) glass tape (G-1001 transfer tape, Vitta Corp, Bethel, CT). The interfacial glass layer had a thickness $\approx$ 50 μm, with elastic and thermal properties closely matching those of the adjacent soda-lime glass. This produced an effective bilayer with veneer modulus 70 GPa (soda-lime + interfacial layer) and core modulus 370 GPa, similar to the veneer/core structure of alumina-based all-ceramic crowns. The top surfaces of the glass plates were abraded with grade 600 SiC grit to provide a uniform density of flaw sites for cone crack initiation. Conversely, the bottom surfaces of the alumina plates were polished down to 1 μm finish grit to avoid premature core radial cracking.[8] No delaminations between glass and alumina were observed during fabrication or ensuing indentation, attesting to the strength of the fused bond. The glass/alumina ceramic bilayers were then glued to a polycarbonate slab 12.5 mm thick (Hyzod, AlN Plastics, Norfolk, VA) with a thin (<20 μm) layer of epoxy resin adhesive (Harcos Chemicals, Bellesville, NJ), analogous to cementation onto a dentin base.

Contact testing was carried out in a fatigue testing machine (Model 5500R, Instron Corp, Canton, MA), as previously.[3] However, now various spherical indenters were used: materials, WC and glass (Salem Specialty Ball Company, Canton, CT); radii, r = 1.6, 5, and 12.5 mm. WC spheres showed little sign of any deformation and were simply rotated between tests. On the other hand, glass spheres showed progressive cracking over time, so a new one was used for each test. Cyclic loading was conducted at a frequency 1 Hz, with peak loads from P_m = 60 N up to P_m = 1000 N and fixed minimum load 2 N (the latter to prevent indenter wandering). A drop of water was placed in the contact region prior to testing and constantly replenished until completion of the test, so that the contact-induced cracks were accessible to water at all times during testing. A video camera was set up for side viewing through the glass walls and crack depths c recorded at the deepest points of penetration for each crack type as a function of number of cycles n. Initiation at $n = n_I$ was measured as the first sighting of any specific crack type. In the case of O cracks, this was clear as an initial, abrupt pop-in event. For I cracks, pop-in was less abrupt, and initial sighting was in any case more difficult—partly because they were obscured by the preceding O cracks and partly because they were filled with water. Median cracks were observed only occasionally, and in any case were hard to

DOI 10.1002/jbmb

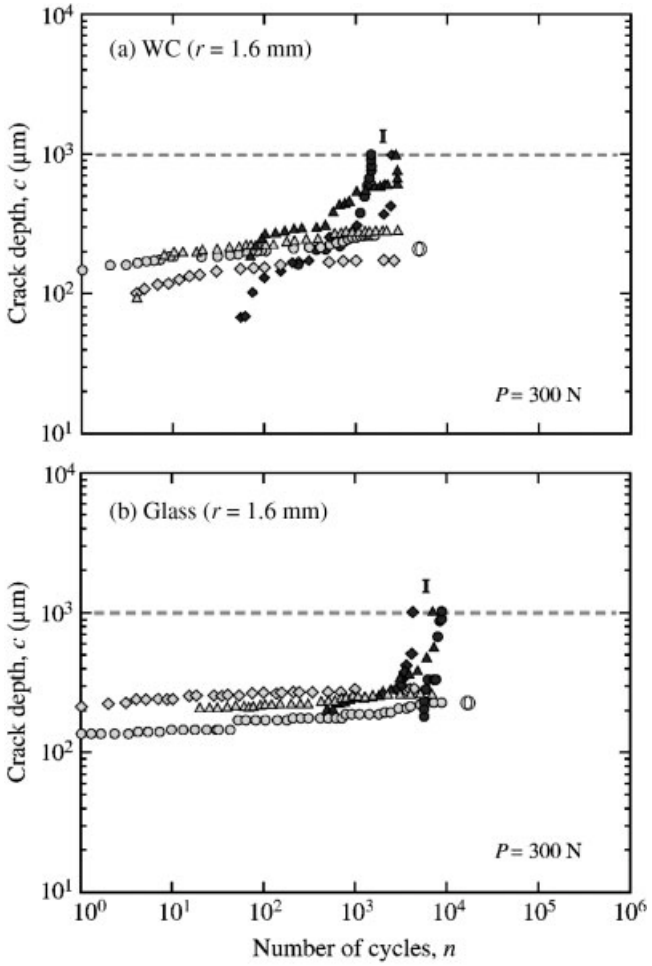

Figure 2. Crack depth c as function of number of cycles n at frequency 1 Hz in water for glass/alumina/polycarbonate trilayers. Indentation with (a) WC and (b) glass spheres of radius $r = 1.6$ mm at fixed peak load $P_m = 300$ N. Data from three tests per indenter (different symbols), showing competition between top-surface cracks in glass layer: outer cone cracks O and inner cone cracks I. Failure occurs when first crack intersects glass/alumina interface (horizontal dashed line).

distinguish from inner cone cracks, so any results from this fracture mode were subsumed into the I crack data. Failure was considered to occur at $n = n_F$ when any one crack fully penetrated the glass layer to reach the interface with the alumina core at $c = 1$ mm. Post-mortem examinations of the failed specimens were made to confirm the absence of any other than top-surface cracks; for example, bottom-surface radial cracks and interface delamination cracks.

RESULTS

Effect of Indenter Material

Figure 2 plots crack depth c in the glass veneer as a function of number of cycles n for (a) WC and (b) glass spheres of radius $r = 1.6$ mm at an intermediate peak load $P_m = 300$ N. The results represent three tests for each indenter. Under these conditions, the outer cone crack O forms within the first cycle and subsequently grows steadily through the upper half of the glass plate. This steady growth has been shown to be entirely consistent with crack extension by moisture-assisted slow crack growth.[1–3] Inner cone cracks I initiate much later in the test, but quickly overtake the outer cones and penetrate through the glass thickness to failure at $c = 1$ mm (horizontal dashed line) after $n_F \approx 10^3$–10^4 cycles. There is an apparent small shift in the data toward longer lifetimes in glass relative to WC indenters.

Figure 3 plots analogous $c(n)$ data for a broad range of maximum loads P_m, using only glass indenters. (Analogous data for WC indenters have been previously reported.[3]) Results are plotted separately for (a) O cracks and (b) I (and M) cracks to avoid data overlap. Failure occurs from O cracks only at high loads, at or above $P_m = 450$ N, after a few cycles. At lower loads, $P_m < 450$ N, most failures occur from I cracks, at greater numbers of cycles. There is considerable scatter in the data, especially for the I cracks, whose mechanics are highly susceptible to variations in initial flaw location and orientation.[9] The principal result in

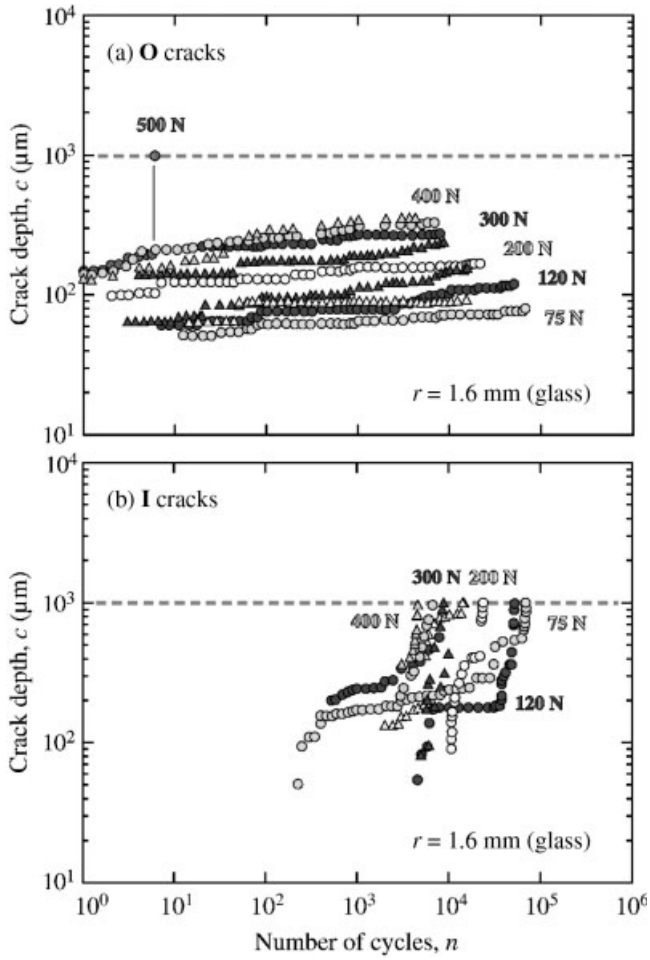

Figure 3. Crack depth c as function of number of cycles n at frequency 1 Hz in water for glass/alumina/polycarbonate trilayers, indentation with glass spheres of radius $r = 1.6$ mm at various peak loads P_m indicated. Data for each cracking mode plotted separately, for clarity: outer cone cracks O and inner cone cracks I.

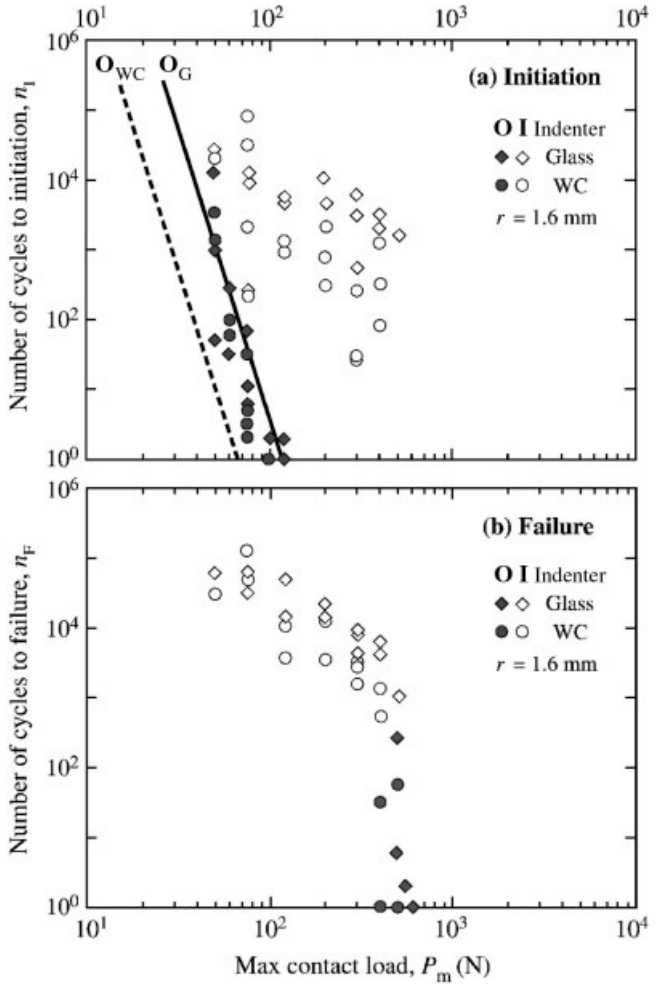

Figure 4. Number of cycles to (a) crack initiation n_I and (b) failure n_F as function of maximum contact load P_m for O mode (filled symbols) and I mode (unfilled symbols), for indentation of glass/alumina/polycarbonate trilayers with WC and glass spheres of radius $r = 1.6$ mm. Lines in (a) are fits to O data using Eq. (1), solid line for glass and dashed line for WC.

these data is the dominance of O cracks at high loads in single- or low-cycle loading and of I cracks at low loads in multicycle loading.

Figure 4 plots critical numbers of cycles for (a) crack initiation, n_I, and (b) failure, n_F, as a function of peak cyclic load P_m for WC and glass spheres of the same radius $r = 1.6$ mm. Individual test data are shown for outer cones (filled symbols) and inner cones (unfilled symbols). The lines are theoretical fits to the O data, the basis of which will be outlined in the Discussion. For the $n_I(P_m)$ plot in Figure 4(a), O cracks always initiate before I cracks, although the gap between the two modes narrows at lower P_m. The scatter in the I data is relatively large, as alluded to above. These initiation data are close to those obtained in an earlier study on monolithic glass using WC indenters,[1] confirming that initiation conditions are dominated by near-field contact stresses. Most important, there appears to be a very slight shift toward higher loads (or longer lifetimes) for the glass relative to WC indenters, although the differences are hardly greater than the scatter in data. For the $n_F(P_m)$ plot in Figure 4(b), O cracks dominate at high loads ($P_m > 450$ N), I cracks dominate at low loads ($P_m < 450$ N). Note that $n_I \ll n_F$ for O cracks [cf. Figure 4(a) with 4(b)], indicating an extended incubation time between

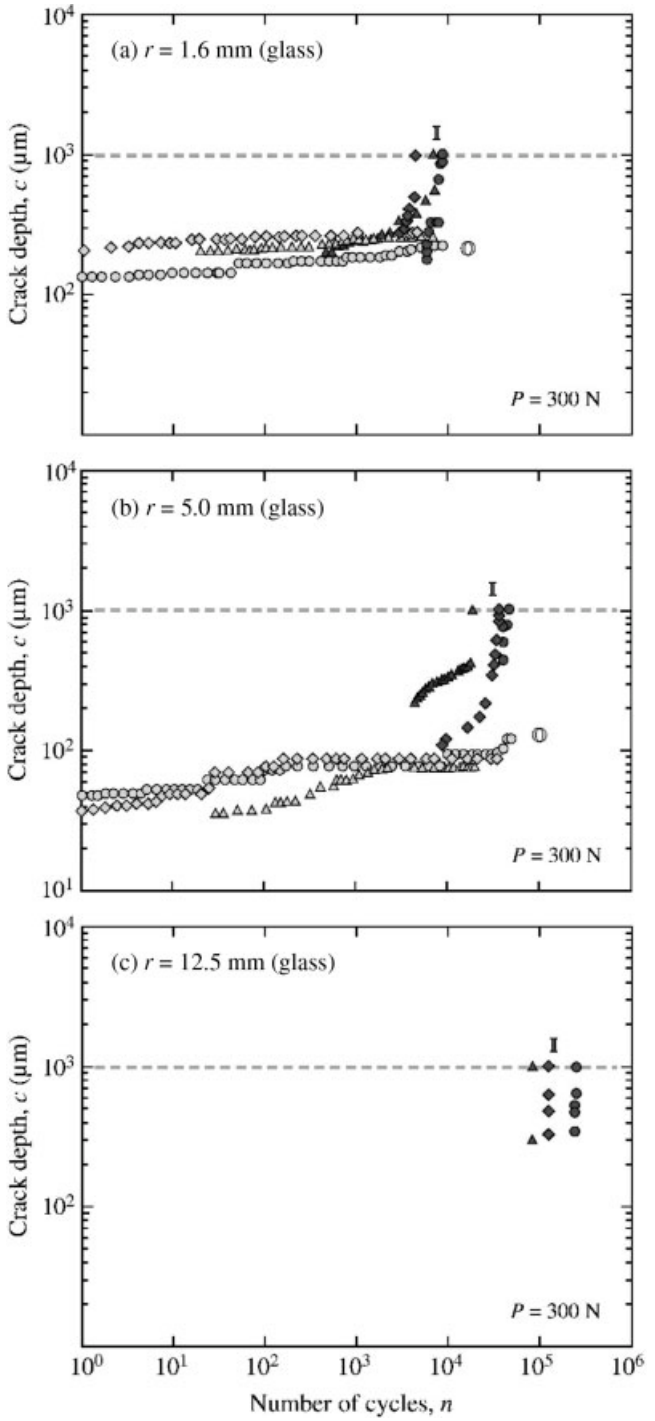

Figure 5. Crack depth c as function of number of cycles n at frequency 1 Hz in water for glass/alumina/polycarbonate trilayers. Indentation with glass spheres of radius (a) $r = 1.6$ mm, (b) $r = 5.0$ mm, and (c) $r = 12.5$ mm at fixed peak load $P_m = 300$ N. Data from three tests per indenter (different symbols), showing competition between outer O and inner I cracks.

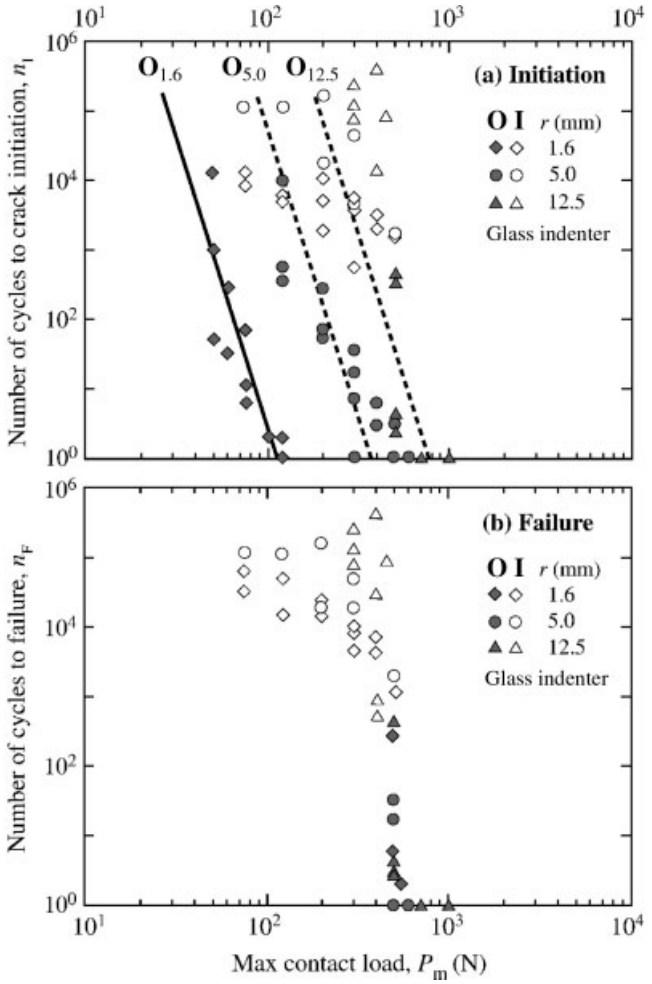

Figure 6. Number of cycles to (a) crack initiation n_I and (b) failure n_F as function of maximum contact load P_m for O mode (filled symbols) and I mode (unfilled symbols), for indentation of glass/alumina/polycarbonate trilayers with glass spheres of radius $r = 1.6$, 5.0, and 12.5 mm. Lines in (a) are fits to O data using Eq. (1), solid line for $r = 1.6$ mm, dashed lines for $r = 5.0$ and 12.5 mm.

first appearance and ultimate penetration of these cracks; but not for I cracks, indicating a much more rapid acceleration to failure, consistent with the data in Figures 2 and 3. The values of n_F for glass and WC spheres now overlap more closely, confirming insensitivity to indenter material, consistent with a far-field-dominated fracture process.[1]

Effect of Indenter Size

Figure 5 compares $c(n)$ data in the glass veneer for indentation with glass spheres of radius (a) $r = 1.6$ mm, (b) $r = 5.0$ mm, and (c) $r = 12.5$ mm at peak load $P_m = 300$ N. The results represent three tests for each indenter. For the smaller radius spheres, the outer cone cracks form early and subsequently grow steadily within the upper half of the glass plate. Inner cone cracks become apparent at $n_I = 10^4$ cycles and quickly penetrate through the glass thickness to failure. Note a perceptible shift to higher loads and longer lifetimes with increasing radius r. Tests with spheres of $r = 12.5$ mm at this load produce only I cracks, with comparatively rapid acceleration to failure, indicating a less stable fracture evolution.

Figure 6 shows plots of (a) $n_I(P_m)$ for initiation and (b) $n_F(P_m)$ for failure for the three different radius glass spheres. Again, individual test data are for O and I cones (filled and unfilled symbols), lines are theoretical fits to the O data (Discussion). The O cracks dominate at high load and short lifetime, I cracks at low load and long lifetime. For crack initiation in Figure 6(a), there is a distinct shift toward larger P_m and longer n_I with increasing r, even allowing for the scatter in data. For failure in Figure 6(b), the data for different r overlap more closely (except for some apparent divergence in the I crack data at higher n_F), again confirming insensitivity of failure to the contact conditions. Note that the gap between the $n_I(P_m)$ and $n_F(P_m)$ data [cf. Figure 6(a) and 6(b)] diminishes with increasing r, until at $r = 12.5$ mm the gap becomes virtually nonexistent. For these larger indenters most of the cracks failed spontaneously upon initiation, most notably from O cracks at the higher loads. Thus higher cuspal radius can increase the threshold load for crack initiation, but the failure tends to be more catastrophic.

DISCUSSION

This work has examined the role of indenter modulus E_i and radius r on top-surface cone fracture in brittle crown-like trilayer structures consisting of glass (simulating porcelain veneer) fused to alumina (support core) bonded to polycarbonate (dentin base). Tests have been carried out in cyclic loading with peak loads 60–1000 N in water, to simulate characteristic occlusal function. Some strong conclusions emerge from the data. Conditions for failure from cone crack penetration through the veneer layer to the core interface, summarized by the $n_F(P_m)$ data in Figures 4(b) and 6(b), are relatively insensitive to either indenter material or indenter radius. This insensitivity is consistent with fracture mechanics solutions in the far-field region of contact, i.e., in a region where crack dimensions are large relative to the contact radius and the number of cycles for initiation n_I remains small compared to n_F. In our experiments the contact radius is typically 200–300 μm, substantially smaller than the 1 mm glass thickness at failure. The same insensitivity is not apparent in the conditions for crack initiation, Figures 4(a) and 6(a). In these cases the mechanics are governed primarily by the near-contact Hertzian stresses, which in turn depend on r and, to a lesser extent, on E_i, as we will confirm below. These latter trends have been noted previously in studies of crack evolution in monolithic brittle solids.[1]

It will be recalled that Figures 4(a) and 6(a) contained linear data fits to the $n_I(P_m)$ data for O cracks. These fits are obtained from the theory of initiation of traditional cone cracks in monoliths, ignoring any potential effects of the finite glass thickness on the Hertzian stress field. (I

cracks are not so amenable to theoretical analysis, because of the complication of superposed hydraulic pumping forces onto the Hertzian field,[1,10] but show analogous data shifts in Figures 4 and 6.) Analysis begins with the so-called Auerbach's law for the critical initiation load P_I in single-cycle loading ($n = 1$),[11–13]

$$P_I = AkrT_1^2/E_1 \quad (1)$$

where E_1 is modulus and T_1 is toughness (K_{IC}) of the veneer (layer 1 in Figure 1), $k = (9/16)(1 - \nu^2)(1 + E_1/E_i)$ is a term accounting for the role of indenter modulus E_i (with ν = Poisson's ratio), and A is a dimensionless constant. In fatigue loading, the O crack extension is governed by a crack velocity relation, leading to a relation for critical number of cycles to failure as a function of peak load P_m,[1]

$$n_I = (P_I/P_m)^{N/2} \quad (2)$$

In Figures 4(a) and 6(a), the solid lines are calculated inserting $E_i = E_1 = 70$ GPa ($\nu = 0.22$) and $T_1 = 0.6$ MPa $m^{1/2}$ for glass, $N = 17$ for water environment,[1] and adjusting $A = 12.0$ to give a best fit to the baseline data for glass spheres of radius $r = 1.6$ mm. Changing E_i in Figure 4(a) or r in Figure 6(a) is then equivalent to shifting the fitted lines laterally, indicated by the dashed lines. This accounts largely for the shifts to higher P_m in Figure 6 with increasing r, but not so well for the shift to lower P_m in Figure 4 with increasing E_i. In the latter case, the smaller than expected shift for WC relative to glass indenters may be attributed to the existence of friction at the contact interface (zero for indenters of like modulus), which in the case of stiffer indenters can suppress the tensile stresses driving the cone cracks outside the contact, leading to an increase in the critical load.[14]

Let us examine the dependence of veneer cone crack evolution on indenter modulus E_i and radius r a little further. The curves in Figure 7 are plots of load P_I for single-cycle O crack initiation calculated directly from Eq. (1) as a function of (a) E_i at fixed $r = 5.0$ mm and (b) r at fixed $E_i = 70$ GPa. The horizontal dashed line at $P_F = 600$ N represents the limiting case of failure from pre-initiated O cracks at $n = 1$ [see Figures 4(b) and 6(b)]. For the $P_I(E_i)$ plot in Figure 7(a), the points represent the two indenter materials used in the present study. The vertical dashed line indicates the condition for like indenter (glass, tooth enamel) and veneer (glass, porcelain) materials. Note that P_I is relatively insensitive to modulus in the stiff-indenter region $E_i > 70$ GPa (maximum factor of two variation), but is strongly sensitive to modulus in the compliant-indenter region $E_i < 70$ GPa. Note also that $P_I > P_F$ for $E_i < 25$ GPa approximately, indicating that fracture initiation with soft indenters will immediately lead to catastrophic failure, albeit at comparatively high loads. In extreme cases of very soft materials such as food bolus, top-surface cone cracks (and even bottom surface radial cracks) can become totally suppressed and alternative modes activated at the specimen margins, the more so in dome-like specimens resembling crown structures.[7]

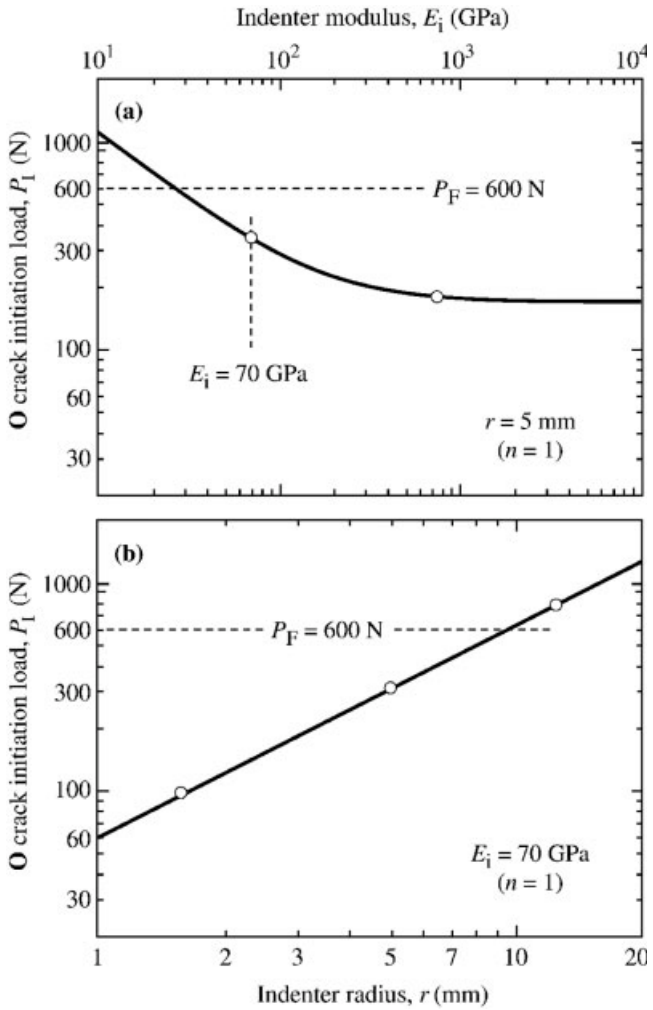

Figure 7. Critical loads P_I to initiate O cone cracks in glass layer in single-cycle loading calculated from in Eq. (1): (a) as function of indenter modulus E_i, at fixed radius $r = 5.0$ mm; (b) as function of r, at fixed $E_i = 70$ GPa. Dashed lines at $P_F = 600$ N indicate failure load.

For the $P_I(r)$ plot in Figure 7(b), the points represent indenter radii used in the present experiments. The dependence is linear in accordance with Auerbach's law, the validity of which is dependent on the availability of prepresent (abrasion) flaws.[15] Again, note that $P_I > P_F$ for $r >$ 10 mm approximately, so that initiation with large spheres will cause immediate penetration through the veneer layer. It has been asserted that curvatures up to 20 mm may be more representative of actual molar occlusal function, so this latter region is pertinent.[5] Notwithstanding this tendency to more catastrophic failure, maintaining large cuspal radii as well as avoiding hard opposing materials would appear to be desirable design goals, to circumvent near-contact crack initiation in the first place.

One issue that is often raised in the clinical context is that of failure of a brittle veneer by single-cycle overload versus cyclic low-load fatigue. Single-cycle overload is equivalent to translating along the horizontal axis $n = 1$ in Figures 4 and 6. Fracture then occurs from O cracks, which initiate at $P_m = P_I$ [Figures 4(a) and 6(a)] and grow steadily

downward through the veneer with increasing load until failure occurs at $P_m = P_F$ [Figures 4(b) and 6(b)]. But in such cases the failure loads are high, $P_F = 600$ N for our glass veneer thickness of 1 mm. This would require an uncommonly severe occlusal event to trigger failure, for instance from inadvertent biting on a hard nut or grit particulate. Fatigue failure is equivalent to translating along a vertical line $P_m = \text{const}$. Failure can then occur at much lower loads and, as apparent from Figures 4 and 6, is then more likely to occur from more deleterious I cracks.[3]

REFERENCES

1. Zhang Y, Bhowmick S, Lawn BR. Competing fracture modes in brittle materials subject to concentrated cyclic loading in liquid environments: Monoliths. J Mater Res 2005;20:2021–2029.
2. Bhowmick S, Zhang Y, Lawn BR. Competing fracture modes in brittle materials subject to concentrated cyclic loading in liquid environments: Bilayer structures. J Mater Res 2005;20: 2792–2800.
3. Hermann I, Bhowmick S, Zhang Y, Lawn BR. Competing fracture modes in brittle materials subject to concentrated cyclic loading in liquid environments: Trilayer structures. J Mater Res 2006;21:512–521.
4. McLean JW. The Science and Art of Dental Ceramics, Vol. 1: The Nature of Dental Ceramics and Their Clinical Use. Chicago: Quintessence; 1979.
5. Kelly JR. Clinically relevant approach to failure testing of all-ceramic restorations. J Prosthet Dent 1999;81:652–661.
6. Lawn BR, Pajares A, Zhang Y, Deng Y, Polack M, Lloyd IK, Rekow ED, Thompson VP. Materials design in the performance of all-ceramic crowns. Biomaterials 2004;25:2885–2892.
7. Qasim T, Ford C, Bush MB, Hu X, Malament KA, Lawn BR. Margin cracks in brittle dome structures. J Biomed Mater Res B. In press.
8. Deng Y, Miranda P, Pajares A, Guiberteau F, Lawn BR. Fracture of ceramic/ceramic/polymer trilayers for biomechanical applications. J Biomed Mater Res A 2003;67:828–833.
9. Chai H, Lawn BR. Hydraulically pumped cone fracture in bilayers with brittle coatings. Scr Mater 2006;55:343–346.
10. Chai H, Lawn BR. Hydraulically pumped cone fractures in brittle solids. Acta Mater 2005;53:4237–4244.
11. Frank FC, Lawn BR. On the theory of Hertzian fracture. Proc R Soc Lond A 1967;299:291–306.
12. Peterson IM, Pajares A, Lawn BR, Thompson VP, Rekow ED. Mechanical characterization of dental ceramics using Hertzian contacts. J Dent Res 1998;77:589–602.
13. Kim DK, Jung Y-G, Peterson IM, Lawn BR. Cyclic fatigue of intrinsically brittle ceramics in contact with spheres. Acta Mater 1999;47:4711–4725.
14. Johnson KL, O'Connor JJ, Woodward AC. The effect of indenter elasticity on the Hertzian fracture of brittle materials. Proc R Soc Lond A 1973;334:95–117.
15. Langitan FB, Lawn BR. Hertzian fracture experiments on abraded glass surfaces as definitive evidence for an energy balance explanation of Auerbach's law. J Appl Phys 1969;40: 4009–4017.